J Mater Sci (2009) 44:4874–4882
DOI 10.1007/s10853-009-3743-x

Characterization and photocatalytic activity of TiO_2–M_xO_y (M_xO_y = SiO_2, Al_2O_3, and ZrO_2) mixed oxides synthesized by microwave-induced solution combustion technique

Benjaram M. Reddy · Gunugunuri K. Reddy · Komateedi N. Rao · Ibram Ganesh · Jose M. F. Ferreira

Received: 12 April 2009 / Accepted: 11 July 2009 / Published online: 29 July 2009

Abstract Titania–silica, titania–alumina, and titania–zirconia mixed oxides (1:1 molar ratio) were prepared by a microwave-induced solution combustion synthesis technique. The prepared materials were characterized by thermogravimetry/differential thermal analysis, X-ray diffraction (XRD), Raman spectroscopy, BET surface area, X-ray photoelectron spectroscopy (XPS), ultraviolet–visible diffuse reflectance spectroscopic (UV–Vis DRS), and Fourier transform infrared (FTIR) techniques to assess their physicochemical properties. Their photocatalytic activity for the degradation of phenol in aqueous solution under sunlight was studied. XRD and Raman studies revealed the presence of titania in the form of anatase phase in all the mixed oxides synthesized. The XRD studies further suggested that titania–zirconia contains an additional (Ti,Zr)O_2 phase. UV–Vis DRS results reveal that all samples exhibit absorption maxima near visible region. FTIR results revealed the presence of Ti–O–Si linkages in the titania–silica sample, which are responsible for its higher activity in the photocatalytic degradation of phenol under sunlight.

B. M. Reddy (✉) · G. K. Reddy · K. N. Rao
Inorganic and Physical Chemistry Division, Indian Institute of Chemical Technology (IICT), Uppal Road, Hyderabad 500607, India
e-mail: bmreddy@iict.res.in

I. Ganesh
Centre for Advanced Ceramics, International Advanced Research Centre for Powder Metallurgy and New Materials (ARCI), Balapur (PO), Hyderabad 500005, India

J. M. F. Ferreira
Department of Ceramics and Glass Engineering, CICECO, University of Aveiro, Aveiro 3810193, Portugal

Introduction

In the field of catalysis, there is a growing interest on the preparation of mixed metal oxides for exploitation, either as catalysts or as catalyst supports [1–3]. The degree of mixing and the textural properties of the mixed oxides are highly influenced by the preparation methodology [1]. Sol–gel [4], metal oxide chemical vapor deposition [5], co-precipitation [6], micro emulsion [7], hydrolysis in polyol medium [8], and decomposition of the precipitates obtained by non-aqueous precipitation method [9] are some of the common preparation routes. Among these methods, sol–gel hydrolysis is most widely used due to its promising capability in controlling the textural and surface properties of the powders. However, in the sol–gel process, domain formation due to the differences in the hydrolysis and the condensation rates of metal ions such as Ti- and Si-alkoxides has been identified as a major problem in the preparation of atomically homogeneous mixed metal oxides. Furthermore, all the wet chemical methods in general, to some extent, still need calcination at relatively high temperatures along with longer duration of soaking to produce the powders with good crystallinity. Since raising the calcination temperature and prolonging the soak time makes the crystalline grains grow larger in size and weaken the reactivity, obtaining nanosized particles has been difficult. Furthermore, powders formed in these methods are highly agglomerated. Recently, combustion synthesis has emerged as an effective powder synthesis route, which is simple and economical. This process does not require any acid or base to hydrolyze the corresponding salts, and additional washing, filtration, drying, and calcination steps can be eliminated, which in turn leads to conservation of time and energy [10, 11]. Of late, microwave energy has been effectively used in the field of materials science for

the synthesis of various single and composite ceramic powders at far lower temperatures and shorter time periods compared to the conventional methods [12, 13]. Since, microwaves interact with reactants at molecular level, reactions normally occur at faster rates, easily, and homogeneously to form the products with much higher yields and superior properties. Microwaves have also been used to induce the solution combustion reactions conducted in domestic microwave ovens, which operate at 2.45 GHz frequency (1 kW).

Of the pure oxides that have been mixed to improve their surface areas while trying to use their chemical properties, titania has been widely studied. It is a reducible oxide of great interest because of its numerous applications, such as photocatalyst and catalyst support, white pigment for paints, cosmetics, fillers, battery electrodes, capacitors, and solar cells. Current progress in the area of TiO_2 applications refer to the photocatalytic air purification, sterilization, and cancer therapy [14]. Among the advantages of titania over other photocatalysts is its excellent (photo) chemical stability, low cost, and nontoxicity can be cited. In particular, titania anatase has been extensively used for several photocatalytic reactions for elimination of many organic pollutants from wastewaters [15, 16]. Anatase TiO_2 is thermodynamically metastable and can be easily transformed into the stable rutile phase when it is heated to 500–600 °C. Furthermore, the anatase to rutile phase transformation is accompanied with a severe sintering or growth of TiO_2 crystallites, which is not preferred for photocatalysis, as there are more chances for recombination of photo-generated electrons and holes in larger crystalline materials. Thus, it is practically important to develop methods that can lead to a stabilization of anatase TiO_2 at higher temperatures, so that the phase transformation in the later thermal treatment can be avoided. The phase transformation can be retarded by doping a metal into the titania or combining the titania with another metal oxide. Examples of mixed oxides include the combination of TiO_2 with SiO_2, ZrO_2, or Al_2O_3. These combined metal oxide materials result in new reactivity properties and higher activity when compared with the solitary metal oxide [17–19].

In view of the above, and considering the importance of titania anatase-based mixed oxides such as, TiO_2–SiO_2, TiO_2–Al_2O_3, and TiO_2–ZrO_2 for photocatalytic reactions, the microwave-induced combustion synthesis route is employed to prepare these three combination oxides and studied their performance as photocatalysts for degradation of phenol in aqueous suspension under sunlight. The structural properties of these three mixed oxides were characterized by using X-ray diffraction (XRD), Raman, Fourier transform infrared (FTIR), X-ray photoelectron spectroscopy (XPS), ultraviolet–visible diffuse reflectance spectroscopic (UV–Vis DRS), thermogravimetry/differential thermal analysis (TGA/DTA), and BET surface area techniques.

Materials and methods

Materials synthesis

The TiO_2–SiO_2, TiO_2–Al_2O_3, and TiO_2–ZrO_2 mixed oxides (1:1 molar ratio) were prepared by microwave-induced solution combustion synthesis method [10, 11]. In a typical experiment, a mixture solution containing requisite quantities of titanyl nitrate ($TiO(NO_3)_2$) formed by the reaction of titanium iso-propoxide with nitric acid, as received zirconyl nitrate ($ZrO(NO_3)_2$) (Loba-Chemie, GR grade, Mumbai, India), and urea (Loba-Chemie, GR grade) was taken in a Pyrex glass dish (150-mm diameter and 80-mm height) and was irradiated with microwaves in a modified domestic microwave oven (BPL India Limited, Bangalore, India, Model no.: BMO-700T, microwave 700 W, input range 210–230 V AC, 50 Hz, microwave frequency 2.45 GHz) to produce TiO_2–ZrO_2 mixed oxide material. In the case of TiO_2–SiO_2, a mixture solution of titanyl nitrate, siliconyl nitrate formed by the reaction of tetraethyl orthosilicate (TEOS) with nitric acid, and urea, and in the case of TiO_2–Al_2O_3, a mixture solution of titanyl nitrate, aluminum nitrate nona-hydrate ($Al(NO_3)_3{\cdot}9H_2O$) (Loba-Chemie, GR grade), and urea were taken as starting materials. A provision was made for the escape of combustion gases by providing an exhaust opening at the top of the microwave oven. Within a few minutes of irradiation, reaction mixture was converted into a clear solution and started boiling, and after about 20 min of irradiation white fumes consisting of N_2, CO_2, and H_2O along with some small traces of NH_3 and NO_2 (confirmed by the odor and color, respectively) started coming out from the exhaust opening provided on the top. After about 45 min of irradiation, the concentrated mixture solution burst into flames and resulted into a foamy white powder. In each case, the entire combustion process took about 60 min to produce highly voluminous mixed oxide powders. Three to four experiments were conducted under identical conditions to check the reproducibility of the present process. Properties of all the synthesized powders were found to be identical. TiO_2–SiO_2, TiO_2–Al_2O_3, and TiO_2–ZrO_2 mixed oxides obtained by the microwave-induced solution combustion process are termed henceforth as MWTS, MWTA, and MWTZ, respectively.

Materials characterization

Powder XRD patterns were recorded on a Bruker (Karlsruhe, Germany) D8 advanced system using a diffracted

beam monochromated Cu $K\alpha$ (0.15418 nm) radiation source. The intensity data were collected over a 2θ range of 2 to 80° with a 0.02° step size and using a counting time of 1 s per point. The XRD phases present in the samples were identified with the help of Powder Diffraction File-International Center for Diffraction Data (PDF-ICDD). The average crystallite size of the oxide phases was estimated with the help of Scherrer equation [20]. Raman spectra were recorded on a triple subtractive Jobin Yvon T64000 Raman spectrometer equipped with a liquid-nitrogen-cooled charge-coupled device detector. The emission line at 514.5 nm from the Ar^+ ion laser was focused on the sample under the microscope, with the width of the analyzed spot being about 1 μm. The BET surface areas of powders were determined by N_2 physisorption at liquid N_2 temperature, on a SMART instrument. Prior to analysis, the samples were oven-dried at 393 K for 12 h and flushed with Argon gas for 2 h. The thermogravimetric measurements were carried out on a Mettler Toledo TG-SDTA instrument. The catalyst sample was heated from ambient to 1073 K under nitrogen flow maintaining the heating rate at 10 K min^{-1}. The XPS measurements were made on a Shimadzu (ESCA 3400) spectrometer by using Mg Kα (1253.6 eV) radiation as the excitation source. Charging of catalyst samples was corrected by setting the binding energy (BE) maximum of the adventitious carbon (C 1s) at 284.6 eV. The UV–Vis DRS measurements were performed over the wavelength range 200–700 nm using a GBS-Cintra 10e UV–Vis NIR spectrophotometer with integration sphere diffuse reflectance attachment. Samples were diluted in a KBr matrix by pelletization.

Photo catalytic activity studies

The photocatalytic activities of the mixed oxides were carried out in a batch photoreactor having a cylindrical flask made of Pyrex of ca. 100 mL. Solar experiments were performed during the mid-day period (Hyderabad) at a temperature of ~315 K and the intensity being ~75 Mw m^{-2} (in March and April months). In each experiment, about 25 mL aqueous phenolic solution (1×10^{-4} M concentration) and 50 mg mixed oxide were used. Prior to the illumination under solar light, the suspension was magnetically stirred in the dark for 1 h to establish adsorption–desorption equilibrium at room temperature. To adjust the pH of the solution, dilute H_2SO_4 and NaOH were used. During the solar irradiation, solid catalysts were allowed to suspend in the solution using a shaking machine (~120 rpm) and distilled water was added periodically to avoid concentration changes due to evaporation. The samples were drawn at specific time intervals through 0.2 μm micro-syringe filters (Millipore millex PVDF, 13 nm, Billeria, MA) to remove particulate matter before high performance liquid chromatography (HPLC) analysis. Phenol degradation was monitored using Shimadzu 10-AvP HPLC equipped with a reverse-phase (length 250 mm; i.d. 4.6 mm) C-18 column with mobile phase acetonitrile/water (50/50 v/v%) and the flow rate was 1 mL min^{-1}.

Results and discussion

Reaction stoichiometry

The high temperatures required for the formation of ceramic powders are usually accomplished by the exothermicity of the redox reactions occurring between the decomposition products of metal nitrate (oxidizer) and urea/carbohydrazide/sucrose (fuel) during combustion [12, 13]. Stoichiometric compositions of the metal nitrates and urea were calculated using the total oxidizing and reducing valencies of the components which provide as numerical coefficients for stoichiometric balance so that the equivalent ratio is unity and the energy generated by the combustion is at a maximum. According to the concepts used in propellant chemistry, the elements Ti, Zr, Al, C, and H have reducing valencies of +4, +4, +3, +4, and +1, respectively. Oxygen has an oxidizing valency of −2 and the valency of nitrogen is zero [21, 22]. Thus, the oxidizing and the reducing valencies of titanyl nitrate, siliconyl nitrate, zirconyl nitrate, aluminum nitrate non-ahydrate, and urea become −10, −10, −10, −15, and +6, respectively.

To prepare MWTS, MWTZ, and MWTA mixed oxides by microwave-induced solution synthesis method using urea as a fuel, $TiO(NO_3)_2$ can be used as Ti source (total valency 10) and $SiO(NO_3)_2$, $ZrO(NO_3)_2$, and $Al(NO_3)_3 \cdot 9H_2O$ as Si, Zr, and Al sources (total valencies 10, 10, and 15), respectively. Direct use of the propellant chemistry criterion [23, 24], with both the metal nitrates, to determine the urea needed to balance the total oxidizing and reducing valencies in the mixture of oxidizers and fuels to prepare titania–silica mixed oxide, leads to $(-10) + (-10) + 6n = 0$. This equation gives $n = 3.33$ moles, which means 3.33 moles of urea is required to prepare one mole of titania–silica (1:1 molar ration) mixed oxide. Similarly, the urea required for the preparation of one mole of titania–zirconia and titania–alumina binary oxides is 3.33 and 4.66 moles, respectively. Assuming complete combustion, the theoretical equations for the redox reactions between metal nitrates and urea for each mixed oxide can be expressed as follows:

TiO_2–SiO_2:

$$TiO(NO_3)_2 + SiO(NO_3)_2 + 3.33NH_2CONH_2 \rightarrow TiO_2{-}SiO_2 + 5.33N_2\uparrow + 3.33CO_2\uparrow + 6.66H_2O\uparrow$$

TiO_2–ZrO_2:

$$TiO(NO_3)_2 + ZrO(NO_3)_2 + 3.33NH_2CONH_2 \rightarrow TiO_2{-}ZrO_2 + 5.33N_2\uparrow + 3.33CO_2\uparrow + 6.66H_2O\uparrow$$

TiO_2–Al_2O_3:

$$TiO(NO_3)_2 + Al(NO_3)_3{\cdot}9H_2O + 4.66NH_2CONH_2 + 3O_2(\text{from air}) \rightarrow TiO_2{-}Al_2O_3 + 7.16N_2\uparrow + 4.66CO_2\uparrow + 18.32H_2O\uparrow$$

Characterization of materials

To study the thermal stability of the mixed oxides and to know about phase transformation from anatase to rutile phase, the as-synthesized mixed oxides were subjected to TGA-DTA analysis between 323 and 1273 K (Fig. 1). As can be noted from this figure, a total weight loss along the whole temperature range tested for MWTS is 13%, whereas for MWTA and MWTZ, it is 23 and 12%, respectively. Decomposition of unreacted metal nitrates and urea, and the loss of absorbed moisture could be responsible for the noted weight losses. There are two stage weight losses; the first stage is from room temperature to 423 K, which is caused by loss of physically absorbed moisture on the surface of the sample. The second stage is from 423 to 673 K, where urea and metal nitrates underwent decomposition in the temperature range 427–636 K; this endothermic process is accompanied with a large weight loss and vigorous gas emission. Thus, the possible decomposition of unreacted urea/nitrates could contribute according to the literature data [25], to weight loss in the TGA and to endothermic process in the DTA. The weight loss beyond 673 K was about 0.5% for all samples, indicating that over the temperature range of 673 to 1073 K, the mixed oxides are quite stable in terms of phase and chemical composition. However, Ramirez and colleagues [26] reported that titania–alumina mixed oxide exhibits a very broad exothermic peak in the region between 973 and 1073 K in the DTA curve, which is associated to the anatase-to-rutile phase transformation and a preceding sintering. In this study, no such peak was observed in any of the oxides. This gives an impression that the titania-based mixed oxides formed in the microwave-assisted solution combustion route are quite resistant

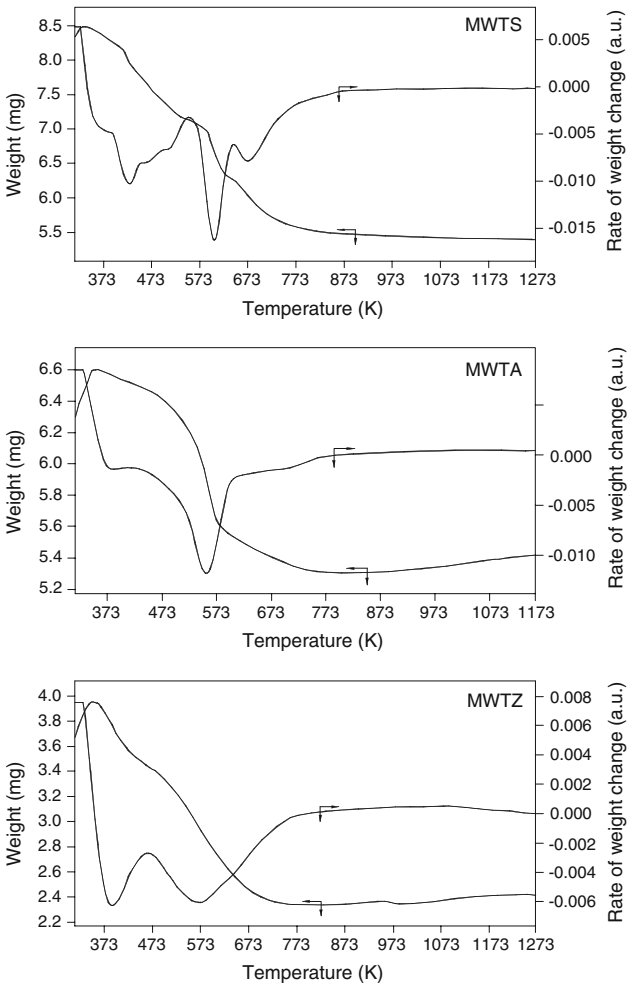

Fig. 1 TGA/DTA thermograms of various TiO_2–M_xO_y mixed oxides (MWTS, TiO_2–SiO_2; MWTA, TiO_2–Al_2O_3; MWTZ, TiO_2–ZrO_2)

Table 1 BET surface area, crystallite size, and edge energy measurements of TiO_2–M_xO_y mixed oxides

Material	BET surface area (m^2/g)	Crystallite size (nm)	Edge energy (eV)
MWTS	115	10	3.2
MWTA	94	13.5	3.15
MWTZ	89	15	3.15

MWTS TiO_2–SiO_2, *MWTA* TiO_2–Al_2O_3, *MWTZ* TiO_2–ZrO_2

to phase transformation up to 1073 K [17, 19]. The N_2 BET surface areas of various mixed oxides prepared are represented in Table 1. All the samples exhibit reasonably high surface areas. As expected titania–silica sample exhibits very high surface area compared to other samples. This may be due to stabilization of nanosized titania particles over the surface of silica. The decreasing order of surface area is MWTS > MWTA > MWTZ.

Figure 2 shows the characteristic XRD peaks of MWTS, MWTA, and MWTZ powders. Peaks essentially due to

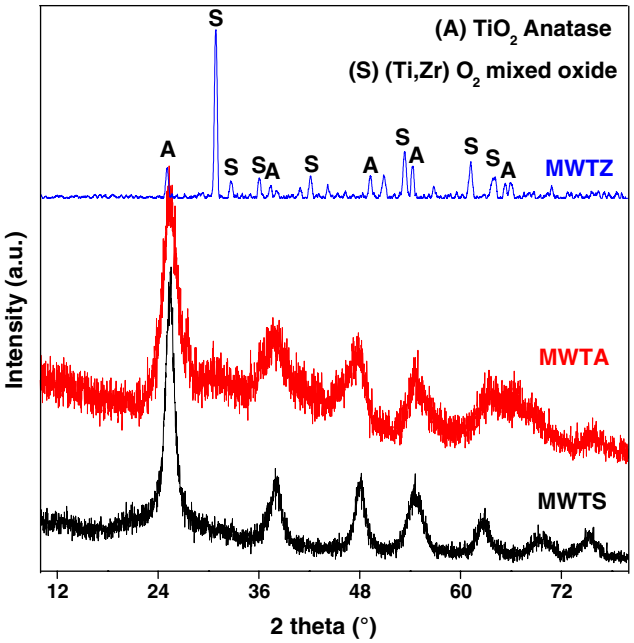

Fig. 2 X-ray powder diffraction patterns of various TiO_2–M_xO_y mixed oxides (MWTS, TiO_2–SiO_2; MWTA, TiO_2–Al_2O_3; MWTZ, TiO_2–ZrO_2)

crystalline anatase phase (JPCDS File no. 21-1272) are seen in the XRD patterns of MWTS and MWTA samples. The most intense anatase peak is present at $2\theta = 25.3°$. In the case of MWTZ, in addition to peaks due to anatase phase, few sharp additional peaks at $2\theta = 30.52$, 53.16, 61.1° are seen, which are attributed to srilankite (Ti,Zr)O_2 (JPCDS File no. 35-0584), a compound formed by the reaction of titania with zirconia. There is a slight shift in the 2θ values of analyzed powders that could be attributed to several reasons such as the differences between the particle sizes of the analyzed powders, preferred orientation of the crystallites, the degree of impurity entered into crystal lattice, depth of scattering of the diffracted radiation, and so on. In our earlier investigation also, the formation of $ZrTiO_4$ was noted in case of titania–zirconia mixed oxide prepared by a conventional coprecipitation method [27]. Thus, the present results are corroborating with earlier reports. Interestingly, no peaks pertaining to rutile phase are exhibited by any of the mixed oxides prepared. However, several authors reported the formation of rutile phase at higher calcination temperatures above 873 K for these mixed oxides [28]. Although temperatures up to 1273 K generate in the solution combustion reactions, no rutile phase is seen in the XRD patterns of any of the mixed oxides prepared. The high homogeneous mixing of reactants in the microwave-induced combustion reactions could be responsible for high stability of titania of these mixed oxides. Interestingly, no peaks are seen even due to silica and alumina in the case of MWTS and MWTA mixed oxides. Absence of peaks due to either monoclinic or tetragonal zirconia in titania–zirconia mixed oxide indicates that most of the zirconia is either in amorphous form or consumed in the formation of (Ti,Zr)O_2 compound. The crystallite sizes of titania in MWTS, MWTA, and MWTZ are also summarized in Table 1. It can be noted that the crystallite size of titania is dependant of the metal oxide added to it. The anatase titania size in all the mixed oxides is in nanometer range. In general, as expected the crystallite size of titania in titania–silica mixed oxide is relatively smaller in comparison to other samples. This may be due to stabilization of the smaller titania particles over the surface of silica.

Raman spectra of MWTS, MWTZ, and MWTA are shown in Fig. 3. In general, the Raman spectrum of TiO_2 is characterized by a strong band at 144 cm^{-1}, three mild intensity bands at 396, 517, and 639 cm^{-1}, and a weak band at 196 cm^{-1}, which can be assigned to the six fundamental vibrational modes of anatase TiO_2 with the symmetries of Eg, Eg, B1g, A1g, B1g, and Eg, respectively [29]. Consistent with XRD data, Raman spectroscopy also provided evidence that all the mixed oxides consist of anatase structures. The peak at 144 cm^{-1} in the case of MWTS was shifted to lower wave numbers. This may be due to formation of Ti–O–Si linkages (conformed from FTIR results). In the case of MWTZ sample, in addition to these peaks there is another peak at 464 cm^{-1}. This may be due to formation of (Ti,Zr)O_2 mixed oxide which corroborate with XRD results. No Raman peaks are noted due to SiO_2 as reported in the literature [30]. According to the literature [31], six Raman active modes (A1g + 3Eg + 2B1g) are expected for *t*-ZrO_2 (space group *P*42/*nmc*). No Raman lines due to ZrO_2 are observed in the MWTZ sample. These

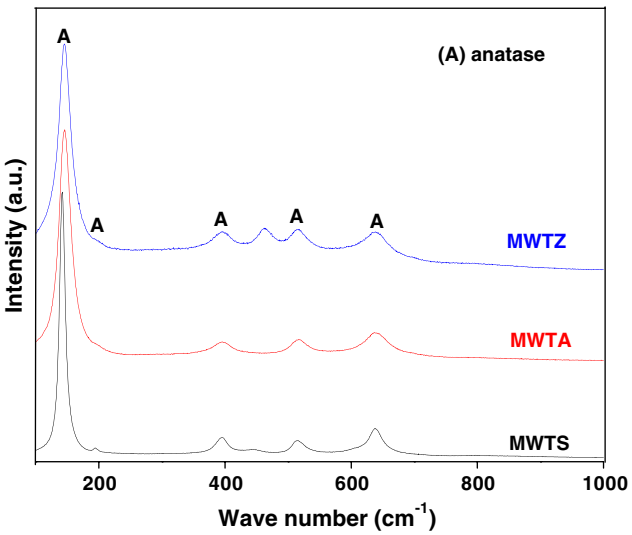

Fig. 3 Raman spectra of various TiO_2–M_xO_y mixed oxides (MWTS, TiO_2–SiO_2; MWTA, TiO_2–Al_2O_3; MWTZ, TiO_2–ZrO_2)

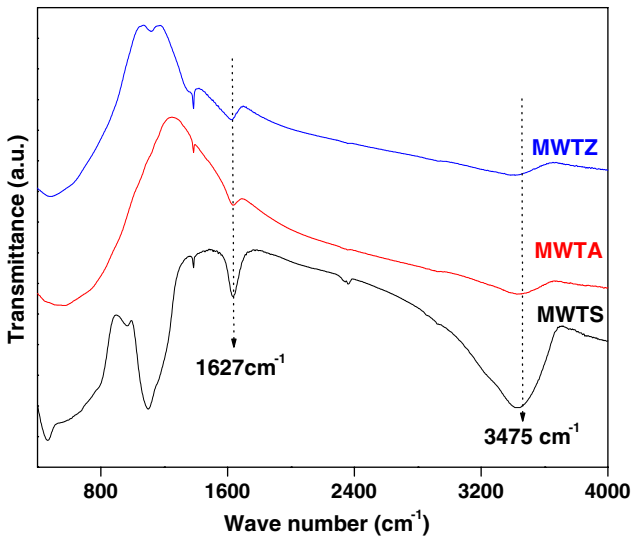

Fig. 4 FTIR spectra of various TiO_2–M_xO_y mixed oxides (MWTS, TiO_2–SiO_2; MWTA, TiO_2–Al_2O_3; MWTZ, TiO_2–ZrO_2)

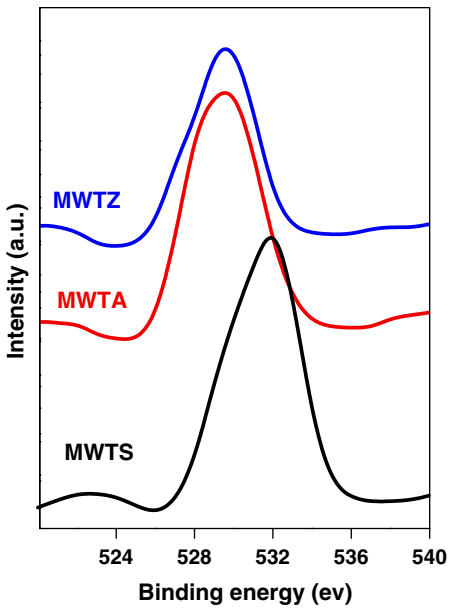

Fig. 5 O 1s XPS spectra of various TiO_2–M_xO_y mixed oxides (MWTS, TiO_2–SiO_2; MWTA, TiO_2–Al_2O_3; MWTZ, TiO_2–ZrO_2)

results indicate that MWTZ does not contain any free ZrO_2 as confirmed from the XRD studies.

FTIR spectra of MWTS, MWTZ, and MWTA are shown in Fig. 4. All the samples exhibit two broad and strong peaks at 3400 and 1625 cm^{-1}. The band at 3400 cm^{-1} could be attributed to stretching vibration of δ (–OH) groups and band at 1625 cm^{-1} is due to bending vibration of the δ (–OH) groups of the Ti–OH and hydrated species [32]. There is a noticeable difference in the intensity of these peaks. These peaks are quite intense in MWTS mixed oxide compared to other samples. The difference in the peak intensities clearly demonstrates that MWTZ and MWTA contain less hydroxyl groups in comparison to MWTS mixed oxide. Additionally, MWTS exhibits another few peaks at 464, 800, 970, and 1098 cm^{-1}. The absorption peaks at 800 and 1098 cm^{-1} were assigned to symmetric ν(Si–O–Si) stretching vibration and asymmetric ν(Si–O–Si) stretching vibration of the SiO_4^{4-} structural unit, respectively [33]. Additionally, the band at 464 cm^{-1} is assigned for Si–O–Si bending modes [34]. It is interesting to note that the peak at 970 cm^{-1} is observed only in the spectrum of MWTS. It is often used as evidence for Ti incorporation into the silica lattice. This band has been ascribed to a vibration involving SiO_4 tetrahedra bonded to a titanium atom through Si–O–Ti bonds. The presence, in the same region, of a band at 970 cm^{-1} arising from Si–OH groups prevents quantitative analysis; however, the high intensity of the 950 cm^{-1} band in our material points to the presence of a large amount of Si–O–Ti linkages [35–37]. It has been reported that the surface hydroxyl groups and Si–O–Ti linkages play an important role in the photodegradation processes through their interaction with photogenerated holes. MWTZ sample exhibits a peak at around 1200 cm^{-1} which may be due to (Ti, Zr)O_2 mixed oxide formation as evidenced by XRD and Raman results.

Table 2 XPS binding energies (eV) of various TiO_2–M_xO_y mixed oxides

Sample	O 1s	Ti 2p	Si 2p	Al 2p	Zr 3d
MWTS	531.8	458.2	103.2	–	–
MWTA	530	458.4	–	73.8	–
MWTZ	530.1	458.6	–	–	182

MWTS TiO_2–SiO_2, *MWTA* TiO_2–Al_2O_3, *MWTZ* TiO_2–ZrO_2

To understand the nature of TiO_2 interaction with ZrO_2, Al_2O_3, and SiO_2, the MWTZ, MWTA, and MWTS samples have been investigated by XPS. The representative XPS bands of O 1s are shown in Fig. 5, and the corresponding BE values are summarized in Table 2. It can be seen that the O 1s profile is, in general, more complicated due to overlapping contributions of oxygen from titania and individual support oxides. As reported in the literature [38–41], the O 1s BE for various single oxides Al_2O_3, SiO_2, ZrO_2, and TiO_2 is 531.4, 532.7, 530.6, and 530.1 eV, respectively. The observed BE values in this study are 531.8, 530, and 530.1 for MWTS, MWTA, and MWTZ mixed oxides, respectively. The O 1s BE values for MWTZ and MWTA are close to the O 1s BE value of pure titania, but in the case of MWTS it is shifted to higher BE. The shift in the BE in case of the latter sample may be due to formation of Ti–O–Si linkages in accordance with FTIR results. The Ti 2p XPS spectra of these three mixed oxides are presented in Fig. 6. All the samples show two shoulder peaks at 458.5 (Ti $2p_{3/2}$)

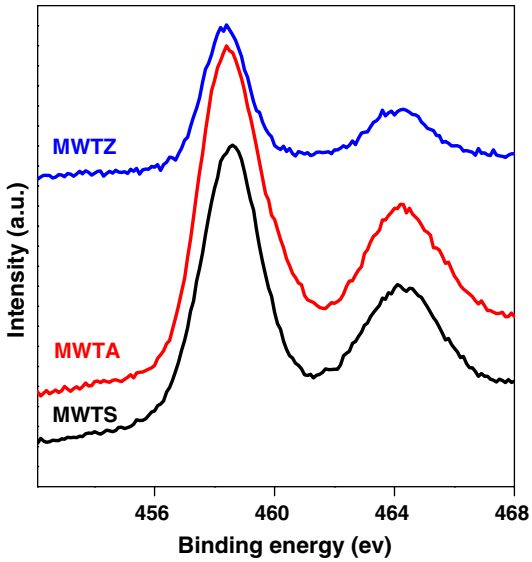

Fig. 6 Ti 2p XPS spectra of various TiO_2–M_xO_y mixed oxides (MWTS, TiO_2–SiO_2; MWTA, TiO_2–Al_2O_3; MWTZ, TiO_2–ZrO_2)

and 464.0 eV (Ti $2p_{1/2}$), respectively. The observed BE values (Table 2) are inline with the literature reports and are also close to that of pure TiO_2 (458.0–458.5 eV) [42–46]. The BE values of Si 2p, Zr 3d, and Al 2p presented in Table 2 are in well agreement with literature reports.

The UV–Vis DRS absorption spectra in the region 200–600 nm were examined to understand the quantized band structure of TiO_2 and the interaction of TiO_2 with other oxides. The band gap of as synthesized samples was calculated from the DRS and presented in Table 1. From the literature, it is known that the absorption edge for titania anatase is around 397 nm and corresponds to the band gap of 3.12 eV. Interestingly, all the materials prepared in the present investigation exhibit red shift by ~20–40 nm compared to the titania anatase [28]. This could be due to the preparation method adopted and presence of foreign oxides. DRS results of all the samples suggest that the absorption edge of the mixed oxides have been moved to the visible spectrum range, which indicates that nanocomposite powders could effectively degrade the phenol under visible light irradiation. However, as we know from literature the photoactivity of the doped TiO_2 catalyst depends substantially on the nature of the dopant ion and its concentration, and method of preparation [47, 48]. Formation of Ti–O–Si linkages and shifting of band gap to visible region in MWTS is an interesting observation from this study.

Phenol mineralization

Photocatalytic degradation of organic pollutants with TiO_2 semiconductor has been proved to be the most efficient process. The effective photo excitation of TiO_2 particles requires the application of light with energy higher than its band gap energy. Moreover, such photo excitation results in the formation of electrons in the conduction band and positive holes in the valence band, and formation of OH radicals [49]. Photo-generated electron–hole pairs also recombine; therefore, inhibiting the recombination of electron–hole pairs and prolonging lifetime of carriers are essential for improving the efficiency of semiconductors. The hydroxyl ions (OH^-) are the likely traps for holes, leading to the formation of hydroxyl radicals that are strong oxidizing agents, while the traps for electrons are adsorbed oxygen species, leading to the formation of superoxide species [50]. The reactive radical species generated (OH^-, O_2^-), attacks the phenolic molecules present in the suspensions and cause its hydroxylation, oxidation, and finally mineralization occurs leading to the formation of carbon dioxide and water [51–53].

Figure 7a displays the phenol degradation profiles of MWTS, MWTZ, and MWTA catalysts at the aqueous pH (6.84). The zero hour indicates the phenol adsorption equilibrium on the catalysts at dark for 1 h. The adsorption of phenol in dark was found to be 68, 55, and 63% for MWTS, MWTA, and MWTZ samples, respectively. As represented in Fig. 7a, the phenol concentration decreases with increasing time. The complete phenol degradation was observed within 3 h of irradiation for all the catalysts. Among the various catalysts, MWTS exhibited highest activity which could be attributed to the high adsorption capacity of phenol on its hydroxyl groups and Ti–O–Si linkages [54, 55]. Even though the adsorption ability of MWTA and MWTZ catalysts was found to be low, after

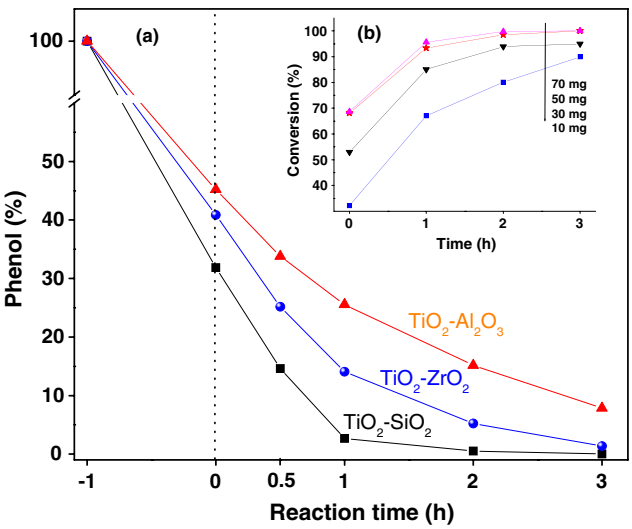

Fig. 7 Phenol degradation profiles of various TiO_2–M_xO_y mixed oxides (MWTS, TiO_2–SiO_2; MWTA, TiO_2–Al_2O_3; MWTZ, TiO_2–ZrO_2)

Table 3 Effect of pH of the phenolic solution on the degradation of phenol over various TiO_2–M_xO_y mixed oxides

Sample	Time (h)	Phenol conversion (%)				
		pH 4	pH 5	pH 6	pH 7	pH 8
MWTS	0	60.49	65.50	67.75	68.13	56.26
	1	82.18	85.48	92.63	97.32	77.84
	2	91.57	90.02	98.87	99.50	92.69
	3	95.12	98.01	99.05	100	97.19
MWTA	0	42.38	48.39	54.24	54.82	35.12
	1	67.93	70.84	76.43	74.44	63.59
	2	78.52	83.20	86.69	84.86	75.75
	3	86.44	90.77	92.88	92.17	82.33
MWTZ	0	58.82	59.98	62.23	63.16	47.02
	1	79.34	80.89	83.85	86.95	77.47
	2	89.63	90.40	95.16	94.76	89.95
	3	92.80	94.10	99.10	98.63	95.47

MWTS TiO_2–SiO_2, *MWTA* TiO_2–Al_2O_3, *MWTZ* TiO_2–ZrO_2

about 3 h of irradiation time, more than 95% phenol conversion was occurred. According to the principles of photocatalysis, the important step of the reaction is the adsorption of reactants on the surface of the solid semiconductor photocatalyst [54]. The rate of reaction is directly proportional to the adsorption capacity of the catalyst. Additionally, high phenol adsorption at dark suggests that the prepared nanocomposite oxides are promising photocatalysts for phenol degradation in the visible light. Tsai and Cheng [55] have reported that between the laboratory-made anatase and rutile TiO_2, anatase titania exhibited better photocatalytic activity for the decomposition of phenolic pollutants. In this study, the XRD results revealed the exclusive formation of anatase phase in all the mixed oxides, thus the present investigation is corroborating well with earlier reports [55, 56]. The increase in the photocatalytic activity of the MWTS is also due to the presence of Ti–O–Si linkages which are conformed by FTIR studies.

Figure 7b shows the effect of MWTS catalyst amount (20, 30, 50, and 70 mg) on the phenol degradation efficiency. It can be seen from Fig. 7b that the optimum concentration of the catalysts is 50 mg, since there is no noticeable increase in the activity when its amount was increased from 50 to 70 mg. These results suggest that the lower amounts of catalyst (30 mg) are not sufficient to absorb the photons entered the reaction cell and the little excess of the catalyst (50 mg) shades the part of the reacting surface of the active catalyst from visible light. A series of experiments were conducted to study the effect of pH of the phenolic solution on the degradation of phenol over MWTS, MWTZ, and MWTA and the results are presented in Table 2. Interestingly at pH = 7, all the mixed oxides exhibited higher degradation activity (Table 3).

Summary

By adopting a simple single-step microwave-induced solution combustion synthesis method, TiO_2–SiO_2, TiO_2–ZrO_2, and TiO_2–Al_2O_3 mixed oxides with sufficiently higher surface areas were prepared. These materials were found to be quite thermally stable (i.e., no phase transformation from anatase to rutile) as revealed by TGA studies. XRD results suggest that TiO_2–SiO_2 and TiO_2–Al_2O_3 contain nanocrystalline anatase titania over the surface of silica and alumina, respectively. In addition to titania anatase phase, formation of $(Ti,Zr)O_2$ mixed oxide was observed in the case of TiO_2–ZrO_2 sample. Raman results also concluded the formation of titania anatase phase. FTIR results revealed the presence of more number of hydroxyl groups and Ti–O–Si linkages in the TiO_2–SiO_2 sample. XPS results indicated that all the elements in TiO_2–SiO_2, TiO_2–ZrO_2, and TiO_2–Al_2O_3 samples were in highest oxidation state. Among the three materials synthesized, the TiO_2–SiO_2 showed highest activity for phenol degradation, which might be due to its higher surface area as well as higher absorption band gap.

Acknowledgements G.K.R. and K.N.R. thank UGC, New Delhi, India, for senior research fellowships. The authors also acknowledge the support of CICECO.

References

1. Miller JB, Ko EI (1997) Catal Today 35:269
2. Gao X, Wachs IE (1999) Catal Today 51:233
3. Dhar GM, Srinivas BN, Rana MS, Kumar M, Maity SK (2003) Catal Today 86:45
4. Dhana S, Malhotra GL, Rastogi AC, Das BK (1992) Thin Solid Films 209:116
5. del Arco M, Trujillano R, Rivers V (1998) J Mater Chem 8:761

6. Lisieechki I, Pileni MP (1993) J Am Chem Soc 115:3887
7. Liu C, Rondinone AJ, Zang ZJ (2002) Pure Appl Chem 72:37
8. Amman G, Arnand H, Jouini N, Fievet F, Rosemann I, Villian F, Milince P, Davot M (2001) J Mater Chem 11:186
9. Sen D, Deb P, Mazumdar S, Basumallik A (2002) Mater Res Bull 35:1243
10. Reddy BM, Reddy GK, Khan A, Ganesh I (2007) J Mater Sci 42:3557. doi:10.1007/s10853-007-1560-7
11. Reddy BM, Reddy GK, Ganesh I, Ferreira JMF (2009) J Mater Sci 44:2743. doi:10.1007/s10853-009-3358-2
12. Palchik O, Zhu J, Gedanken A (2000) J Mater Chem 10:1251
13. Mingos P (1994) Chem Ind 596
14. Rao TN, Tryk DA (2000) J Photochem Photobiol C Photochem Rev 1:1
15. Ollis FD, Al-Ekabi H (eds) (1993) Photocatalytic purification and treatment of water and air. Elsevier Science, Amsterdam
16. Hoffmann MR, Martin ST, Choi W, Bahnemann DW (1995) Chem Rev 95:69
17. Yang J, Huang YX, Ferreira JMF (1997) J Mater Sci Lett 16:1933
18. Yang J, Ferreira JMF (1998) Mater Res Bull 33:389
19. Yang J, Ferreira JMF (1998) Mater Lett 36:320
20. Klug HP, Alexander LE (1974) X-ray diffraction procedures for polycrystalline and amorphous materials, 2nd edn. Wiley, New York
21. Merzanov AG (1993) Int J Self-Propag High-Temp Synth 2:113
22. Ganesh I, Jhonson R, Mahajan YR, Khan A, Madavendra SS, Reddy BM (2004) J Mater Res 19:1015
23. Purohit RD, Sharma BP, Pillai KT, Tyagi AK (2001) Mater Res Bull 36:2711
24. Patil KC, Aruna ST, Ekambaram S (1997) Curr Opin Solid State Mater Sci 2:158
25. Biamino S, Badini C (2004) J Eur Ceram Soc 24:3021
26. Alejandre AG, Trombetta M, Busca G, Ramirez J (1997) Microporous Mater 12:79
27. Reddy BM, Chowdary B, Ganesh I, Reddy EP, Rojas TC, Fernandez A (1998) J Phys Chem B 102:10176
28. Jung KY, Park SB (2004) Mater Lett 58:2897
29. Alonso MDH, Coronado JM, Baeza BB, Garca MF, Soria J (2007) Chem Mater 19:4283
30. Reddy BM, Khan A, Yamada Y, Kobayashi T, Loridant S, Volta JC (2002) J Phys Chem B 106:18751
31. Yashima M, Arashi H, Kakihana M, Yoshimura M (1994) J Am Ceram Soc 77:1067
32. Nagaveni K, Hegde MS, Madras G (2004) J Phys Chem B 108:20204
33. Brinker CJ, Scherer GW (1990) Sol-gel science: the physics and chemistry of sol-gel processing. Academic Press, Boston, MA
34. Lee JW, Kong S, Kim WS, Kim J (2007) Mater Chem Phys 106:39
35. Beck C, Mallat T, Buergi T, Baiker A (2001) J Catal 204:428
36. Klein S, Thorimbert S, Maier WF (1996) J Catal 163:476
37. Dutoit DCM, Schneider M, Baiker A (1995) J Catal 153:165
38. Reddy BM, Chowdary B, Smirniotis PG (2001) Appl Catal A Gen 211:19
39. Biener J, Baumer M, Wang J, Madrix R (2000) J Surf Sci 450:12
40. Galtayries A, Sporken R, Riga J, Blanchard G, Caudano R (1998) J Electron Spectrosc Relat Phenom 88–91:951
41. Reddy BM, Chowdhury B, Reddy EP, Fernandez A (2001) Appl Catal A Gen 213:279
42. Wauthoz P, Ruwet M, Machej T, Grange P (1991) Appl Catal 69:149
43. Mukhopadhyay S, Garofalini S (1990) J Non-Cryst Solids 126:202
44. Wei Z, Xin Q, Guo X, Sham EL, Grange P, Delmon B (1990) Appl Catal 63:305
45. Reddy BM, Ganesh I, Reddy EP (1997) J Phys Chem B 101:1769
46. Briggs D, Seah MP (eds) (1990) Practical surface analysis, auger and X-ray photoelectron spectroscopy, vol 1, 2nd edn. Wiley, New York
47. Lee W, Gao WM, Dwight K, Wold A (1992) Mater Res Bull 27:685
48. Dvoranova D, Brezova V, Mazur M, Malati MA (2002) Appl Catal B Environ 37:91
49. Chen DW, Ray AK (1999) Appl Catal B Environ 23:143
50. Barakat MA, Schaeffer H, Hayes G, Ismat-Shah S (2005) Appl Catal B Environ 57:23
51. Gouvea CAK, Wypych F, Mraes SG, Duran N, Nagata N, Zamora PP (2000) Chemosphere 40:433
52. Debabrata C, Mahata A (2004) J Photochem Photobiol A Chem 165:19
53. Sobczynski A, Duczmal L, Zmudzinski W (2004) J Mol Catal A Chem 213:225
54. Anderson C, Bard AJ (1997) J Phys Chem B 101:2611
55. Tsai SJ, Cheng S (1997) Catal Today 33:227
56. He D, Lin F (2007) Mater Lett 61:3385